

Early hydration of ye'elimitite: insights from thermodynamic modelling

Maciej Zajac¹, Jan Skocek¹, Frank Bullerjahn¹, Barbara Lothenbach², Karen Scrivener³, Mohsen Ben Haha¹

¹Global R&D HeidelbergCement AG, Oberklamweg 2-4, 69181 Leimen, Germany

²Empa, Swiss Federal Laboratories for Materials Science and Technology, Laboratory for Concrete/Construction Chemistry, Überlandstrasse 129, 8600 Dübendorf, Switzerland

³EPFL STI IMX LMC MXG 232 (Bâtiment MXG) Station 12 CH-1015 Lausanne Switzerland

1 Abstract

2 This study focuses on better understanding of early reaction of ye'elimitite, the main constituent of calcium
3 sulfoaluminate cements and the effect of minor phases.

4 Thermodynamic modelling was used to calculate the solubility in the tri-dimensional space of Ca-Al-S-H₂O at
5 different alkali concentrations and compared to changes in the pore solution concentrations during the
6 ye'elimitite reaction. It is demonstrated that the hydration pathways follow the stability fields of certain
7 hydrates. The interplay between the solution properties and the solubility of different phases results in an
8 increase of aluminium, sulfate, and calcium concentrations following the congruent dissolution of ye'elimitite.

9 Moreover, once hydrates start to precipitate, their supersaturation does not change as intensely as the pore
10 solution concentration. This explains the slow reaction of pure ye'elimitite. The same framework was applied
11 to explain fast reaction of ye'elimitite in the industrial clinkers and particularly the effect of C₁₂A₇ and alkalis.

12
13 Key words

14 A Hydration, A Reaction, B Thermodynamic Calculations, B Pore Solution, D Sulfoaluminate, E Modelling

15 1. Introduction

16 Ye'elimitite phase is an important component of calcium sulfoaluminate (CSA) cements. CSA cement has been
17 used in China as the "third cement series" for more than 30 years for construction and special applications
18 [1] [2] and today, the production of CSA cement in China is more than 1 million tonnes per year [3]. Recently,
19 belite-rich CSA cements, so-called belite ye'elimitite ferrite (BYF) cements are gaining increasing attention of
20 cement producers [4][5][6] as a low CO₂ alternative to Portland cement. Despite the long history of the CSA
21 systems use in many applications, the early hydration mechanisms of ye'elimitite clinkers and/or cements are

This document is the accepted manuscript version of the following article:

1

Zajac, M., Skocek, J., Bullerjahn, F., Lothenbach, B., Scrivener, K., & Ben Haha, M. (2019). Early hydration of ye'elimitite: Insights from thermodynamic modelling. *Cement and Concrete Research*, 120, 152-163. <https://doi.org/10.1016/j.cemconres.2019.03.024>

This manuscript version is made available under the CC-BY-NC-ND 4.0 license <http://creativecommons.org/licenses/by-nc-nd/4.0/>

22 not well understood although the understanding of this mechanisms is very important since the hydration of
23 ye'elimites regulates the evolution of the early cement performance [2] [7].
24 With water alone, the hydration of ye'elimites is often idealized according to the simple equation:



25 to form monosulfate and aluminum hydroxide, with the latter being usually X-ray amorphous. The addition
26 of anhydrite modifies the reaction to:



27 According to these reactions, the reaction products are monosulfate or ettringite and aluminium hydroxide
28 in the final product. The content of ettringite and monosulfate is regulated by the ratio between ye'elimites
29 and calcium sulfate. However, many publications [2] [8] [9][10] suggested that the reaction of ye'elimites with
30 water is more complex than these simplified reactions as summarised in. The products of the synthetic
31 ye'elimites reaction include a substantial amount of amorphous CAH₁₀ phase and ettringite in addition to
32 aluminium hydroxide and monosulfate [9][10]. The formation of CAH₁₀ has also been observed in hydrated
33 industrial clinkers and cements [11] [12] [13][14]. The CAH₁₀ phase precipitation is closely linked to the nature
34 of aluminium hydroxide. Aluminium hydroxide has three forms: XRD amorphous, microcrystalline phase or
35 crystalline gibbsite [15] [16] [17]. These forms are characterized by different solubilities, amorphous
36 aluminium hydroxide is the most soluble while gibbsite has the lowest solubility but it generally forms very
37 slowly at room temperature [18]. During the early hydration, the amorphous form of aluminium hydroxide
38 precipitates which stabilizes the CAH₁₀ phase [11] [18] [8]. Later on, when microcrystalline aluminium
39 hydroxide forms, the CAH₁₀ phase is destabilized. Hence, even the hydration of the neat ye'elimites phase is
40 more complex than the idealized reactions (1) and (2). Furthermore, the kinetics of the ye'elimites reaction
41 vary strongly depending on the system investigated. Synthetic, pure ye'elimites reacts slowly [2][9] [19] while
42 ye'elimites in industrial cements may react very rapidly [1] [8][20] [21] [22].

43 Despite considerable research on ye'elimites / CSA hydration, there are few reported studies linking the pore
44 solution properties with the evolution of the solid phases. Such studies are needed for understanding the
45 early hydration mechanisms. Additionally, many of the studies focusing on early hydration investigated

46 cement clinker or cements and using retarders [20] [23] [24], which may interfere with the hydration of the
47 ye'elimit. Consequently, this hinders understanding the mechanisms of early reactions. Additionally, the
48 earliest pore solution extractions reported are too late [20] [25] [26] [19] to capture all the early hydration
49 features as these are typically gained only after few hours after the mixing with water.

50 The two main process that governs the hydration phenomena are dissolution and precipitation [28]. A
51 suitable way to investigate the mechanisms of hydration is to compare the evolution of the pore solution
52 composition resulting from the dissolution of anhydrous phases with the solubility surfaces of hydrates that
53 may precipitate [28] [29]. In this paper, The GEM-Selektor software was applied to investigate the stability
54 of hydrates in the Ca-Al-S-K-H₂O system. The solubility surfaces for the main hydrates which may precipitate
55 during the reaction of ye'elimit were calculated and compared them to the solution data to investigate the
56 mechanisms of ye'elimit hydration, depending on the Ca, Al, S and alkali concentrations in the solution.

57 The thermodynamic modelling of the system Ca-Al-S-H₂O and its sub-systems have been previously
58 investigated by Damidot and Glasser using the state of the art databases available at that time [30] [31] [32].

59 However, the pore solution was treated in a simplified form without considering ion speciation. This is an
60 important aspect since the measured data on the Al, Ca and S concentration vary between μM and hundreds
61 of mM during the hydration of ye'elimit. Additionally, the alkali concentration is typically limited to 0.1 - 1
62 mM in the synthetic systems but can be hundreds of mM in the industrial cements [25]. The use of a modern
63 geochemical software package, GEM-Selector, together with its standard database [33] [34] allows
64 calculation of aqueous ion activities and speciation for the particular system studied. This thermodynamic
65 database has been extended and updated considerably, as summarised in [11][18][35][36] allowing the state-
66 of-the-art modelling.

67 In the present work, the starting point is the simple and relatively well known system Ca-Al-H₂O. It is analysed
68 to explain the early hydration of calcium aluminate cements. In the next sections, more complex systems are
69 presented including gradually the effect of alkalis and sulphate on the Ca-Al-H₂O system. Finally, the Ca-Al-S-
70 K-H₂O system is discussed from the perspective of the reaction of the pure ye'elimit and ye'elimit in a

71 cement clinker in order to consolidate our knowledge on the early hydration of the calcium sulfoaluminate
72 phase.

73 **2. Materials and methods**

74 **2.1. Thermodynamic modelling**

75 Thermodynamic modelling was carried out using the geochemical modelling program GEM-Selector version
76 3.2 [37] [38] with thermodynamic data from the PSI-GEMS database [33] [34] supplemented by cement
77 specific data from the CEMDATA18 database [35][36]. The database compiles thermodynamic data for
78 hydrates such as ettringite, monosulfate and CAH₁₀. The thermodynamic database includes also data for
79 amorphous aluminium hydroxide (Al(OH)₃(am), log K_{SO} = 0.24 for the reaction Al(OH)₃(am) + OH⁻ ⇌ Al(OH)₄⁻
80 [18]), which has a higher solubility than microcrystalline aluminium hydroxide (Al(OH)₃(mic), log K_{SO} = - 0.67
81 for the reaction Al(OH)₃(mic) + OH⁻ ⇌ Al(OH)₄; [35]. The CEMDATA18 database was completed with
82 thermodynamic data for the solubility of ye'elmitte from [39] ($\Delta G^\circ_f = -7929.5 \text{ kJ/mol}$ for Ca₄(Al₆O₁₂)SO₄).
83 GEM-Selector is a broad-purpose geochemical modelling code which computes equilibrium phase
84 assemblage and speciation in a complex chemical system from its total bulk elemental composition. The
85 activity of a species *i*, {*i*}, is calculated with GEM-Selector from the measured concentrations in mol/kg H₂O,
86 *m_i*, considering the formation of aqueous complexes as {*i*} = *m_i*γ_{*i*}, where γ_{*i*} is the dimensionless activity
87 coefficient. The activity coefficients of the aqueous species γ_{*i*} were computed with the built-in extended
88 Debye-Hückel equation with common ion-size parameter *a_i* of 3.67 Å for KOH solutions and common third
89 parameter *b_y* according to Equation 3:

$$\log \gamma_i = \frac{-A_y z_i^2 \sqrt{I}}{1 + B_y a_i \sqrt{I}} + b_y I \quad \text{Equation 3}$$

91 where *z_i* denotes the charge of species *i*, *I* the effective molal ionic strength in mol/kg H₂O, *b_y* is a semi-
92 empirical parameter ($\sim 0.123 \text{ kg H}_2\text{O/mol}$ for KOH electrolyte at 25°C), and *A_y* and *B_y* are P,T-dependent
93 coefficients; at 25°C and 1 bar pressure, *A_y* ≈ 0.5114 and *B_y* ≈ 0.3288. This activity correction is applicable up
94 to approx. 1 M ionic strength.

95 **2.2. Solubility curves and surfaces**

96 This thermodynamic data were used to calculate the solubility of different hydrates under equilibrium
97 conditions as a function of calcium, aluminium, sulphur and potassium concentrations within the system Ca-
98 Al-S-K-H₂O and plotted as lines in 2-dimensional and as surfaces in 3-dimensional plots within the
99 concentration range 0.01 mM to 100 mM. The K⁺ concentration was varied from 1 to 200 mM to assess the
100 effect of pH. The hydrates considered include hemihydrate, gypsum, portlandite, monosulfate, CAH₁₀,
101 C₂AH_{7.5}, C₄AH₁₃, C₃AH₆, gibbsite and amorphous as well as microcrystalline aluminium hydroxide. The limited
102 number of the phases considered was to facilitate and accelerate the calculations. The selection of phases
103 included into the calculations has no impact on the results as interactions neither among the phases nor
104 between phases and the solution were considered.

105 The solubility line or surface for a given phase corresponds to the concentrations at saturation (saturation
106 index SI is 0). The saturation index is defined as:

107
$$SI = \log\left(\frac{IAP}{K_{sp}}\right)$$
 Equation 4

108 where IAP is the ion activity product, i.e. the concentrations of the involved species in the investigated space
109 and K_{sp} is the solubility of the given phase. If the SI is higher than 0, i.e. above the line or surface, the solution
110 is oversaturated, below it (SI < 0) is undersaturated with respect to that specific phase. The undersaturation
111 with respect to the dissolving ye'elimit was calculated as well. However, the solubility of the ye'elimit was
112 decreases by 20 log units to make plotting of its solubility line into graphs with the hydrated phases possible.
113 This was needed since the solubility of ye'elimit is significantly higher than the ones of hydrates. The
114 reduced solubility line is market as Y-20 in graphs.

115 **2.3. Pore solution data**

116 Finally, the calculated solubility curves and surfaces were compared with the available experimental data on
117 the pore solution concentrations. This enables the kinetic path of the early reaction of ye'elimit to be
118 tracked as well as the path through the solubility curves and surfaces of the hydrates based on the evolution

119 of the pore solution. For the reaction of the pure ye'elimitite early age solution data published in [9] were
120 used, where the ye'elimitite hydration was investigated at w/b = 100 and 40 allowing the solution
121 concentrations to be followed during the early reaction. For the reactions occurring in cement clinkers, the
122 pore solution data from Zajac et al. [20] were used, where an industrial BYF clinker had been studied. The
123 clinker contained belite, ye'elimitite and ferrite phase as the main components. In the industrial clinkers
124 ye'elimitite reacts first, while the hydration of belite and ferrite phases occurs only after days of hydration [20]
125 [21] [40].

126 **3. Results and discussion**

127 **3.1. Solubility lines in Ca-Al-H₂O system**

128 The solubility curves of the hydrated phases in the Ca–Al–H₂O and the Ca–Si–H₂O systems have been used to
129 interpret the hydration of the calcium alumina and calcium silicate phases, respectively [41] [28]. The
130 solubility diagram of Ca–Al–H₂O has been used to explain the early hydration of the calcium alumina cement
131 (CAC), and particularly the effect of C₁₂A₇ on the acceleration of the hydration of the CA phase and on the
132 resulting phase assemblage [42] [43]. Upon contact with water, the CA phase from CAC dissolves and the
133 solution concentrations increase with a Ca/Al = 0.5 (as indicated by the dotted CA line in Figure 1). The
134 solution is always supersaturated with respect to aluminium hydroxide as soon as CA starts to dissolve. With
135 ongoing dissolution highlighted by the dotted line, the solution intersects the solubility line of CAH₁₀ phase
136 as shown in Figure 1. However, the slow nucleation of CAH₁₀ and aluminium hydroxide results in a long
137 induction period of the CAC. The presence of small amounts of C₁₂A₇ phase increases the Ca/Al, such that the
138 solution crosses earlier the solubility curve of C₂AH_{7.5} which nucleates and precipitates rapidly, shortening
139 the setting time of the cement.

140

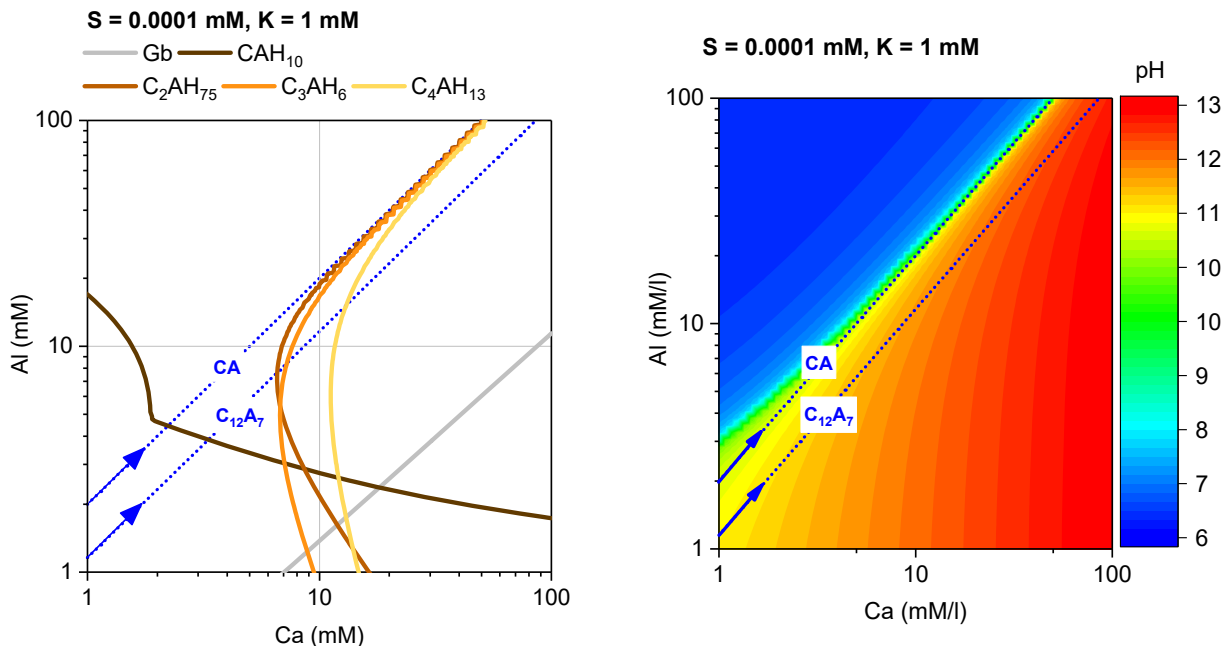


Figure 1 Left: Solubility lines for the relevant hydrates formed during the hydration of CAC, Gb – gibbsite. Below the lines the respective solid is undersaturated and cannot precipitate. Increase of the solution concentration across the line will cause that the hydrate (solid) can form as it is thermodynamically more stable than the solution.

Right: pH map in the calcium alumina plane.

The arrows indicates the direction of the pore solution change during the hypothetical congruent dissolution. The doted lines are showing the evolution of the solution during the hypothetical congruent dissolution of CA and C12A7 phases. For this simulation, low S concentration of 0.0001 mM and K equal to 1 mM was used.

141

142 **3.2. Effect of sulphur and alkali on the solubility relationships in the Ca – Al – H₂O system**

143 In principle, this kind of graph and analysis can also be used for the examination of the hydration of ye'elimito
 144 since it enables the solubility lines of the hydrates involved including ettringite (Et), monosulfate (MS),
 145 aluminium hydroxide (AH₃), CAH₁₀, C₂AH_{7.5}, C₃AH₆ and C₄AH₁₃, to be plotted at any sulphur concentration.
 146 However, this type of graph cannot be used to visualise varying sulphur concentrations or the effect of alkalis.
 147 The dissolving ye'elimito releases three different elements into the solution: Ca, Al and sulphur. Their
 148 speciation (Ca²⁺; CaOH⁺, ...) changes depending on solution concentrations, which increase during the
 149 dissolution of ye'elimito. The effect of sulphur concentration is intuitive for the ettringite and monosulfate
 150 phases, since they contain sulphur. However, sulphur has an even more pronounced effect on other, sulfate-

151 free, phases because of the complex interactions within the pore solution as shown in Figure 2. Similarly, the
152 presence of the alkalis in the system has an effect on the ion speciation, ionic strength of the solution and
153 pH which modifies the solubility lines and surfaces calculated for a given scenario. In this section, both these
154 effects are illustrated and discussed. Note that OH^- is not a free variable as its concentration is determined
155 by the concentration of Ca, Al, S and alkalis, if present, and the global charge balance.

156 In Figure 2 the solubility lines in the Ca – Al plane are compared for two sulphur concentrations. The solubility
157 lines of three hydrates important for the hydration of ye'elinite: aluminium hydroxide (amorphous and
158 gibbsite), CAH_{10} and ettringite, are plotted in the calcium – alumina plane in Figure 2 for sulphur
159 concentrations of 0.1 mM (solid lines) and 1 mM (dashed lines). It is obvious that the sulphur concentrations
160 influence the solubility lines of all hydrates:

161 • aluminium hydroxide (Figure 2 Left): the shape of the curves depends on the sulphur concentration for
162 total Ca and Al concentration lower than 10 mM. It is noticeable that:

163 ○ At lower sulphur concentration, the solubility of aluminium hydroxide increases with increasing Ca
164 concentration as this increases the pH. At the higher sulphur concentration (which lowers the pH)
165 the curves are not monotonic. Alumina solubility decreases with increasing calcium up to ~ 0.5 mM,
166 while Ca concentrations > 0.5 mM solubilise aluminium hydroxide.

167 ○ At the lower sulphur concentration, the amorphous form of aluminium hydroxide is always in
168 equilibrium with much higher aluminium concentration than gibbsite. However, at $S = 1$ mM and
169 lower Ca concentration, the difference in the aluminium concentration between the two forms
170 becomes small.

171 ○ At Ca and Al above 10 mM, the sulphur concentration has little impact on the solubility lines of
172 either polymorph of aluminium hydroxide.

173 • Ettringite (Figure 2 Right): The increasing sulphur concentration results in a shift of the solubility line at
174 lower calcium and aluminium concentrations, while at higher Al and Ca concentrations, the increasing S
175 concentration results only in a slight increase of the ettringite solubility line. It is worth noticing, that the
176 curved solubility lines of ettringite is in equilibrium with two different aluminium concentration at calcium

177 concentrations above 2 mM, which is counter intuitive; i.e. a vertical line at Ca concentration = 5mM
178 would cross the solubility line twice.

179 • The increasing sulphur concentration increases the solubility of the CAH₁₀ (Figure 2 Right) phase in the
180 range of Ca concentrations 0.1 to ~ 3 mM. At the other Ca concentrations, the S concentration has limited
181 impact (within the investigated range).

182

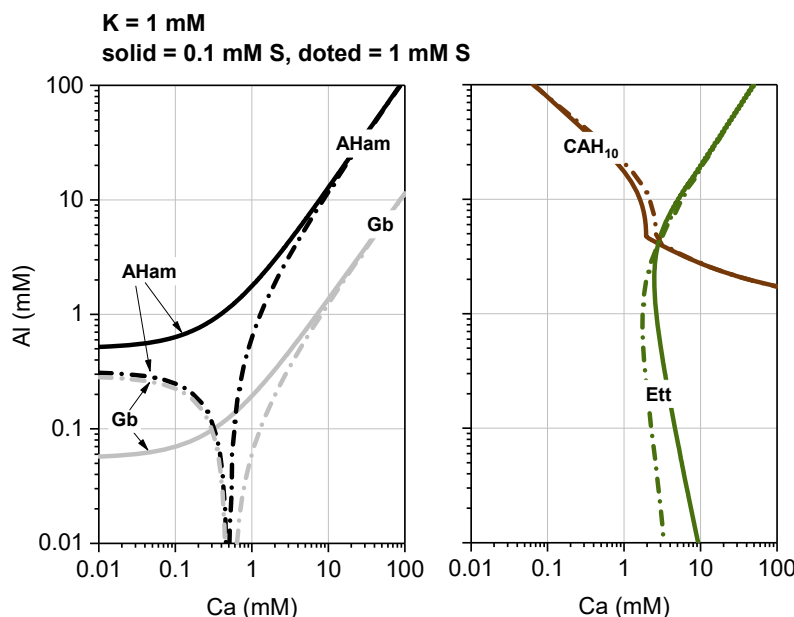


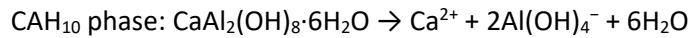
Figure 2 Solubility lines at different sulphur concentrations: CAH₁₀ - CAH₁₀ phase, Ett – Ettringite, Gb – gibbsite, AHam - aluminium hydroxide amorphous. The lines are showing the transition from liquid to solid. Increase of the solution concentration across the line will cause that the hydrate (solid) is more thermodynamically stable than the solution. The solid line shown the calculation results at 0.1 mM of S, and dotted at 1 mM of S. K concentration is 1 mM for both cases.

183

184 The evolutions observed have two explanations, depending on the chemical composition of the hydrates:
185 ○ For the hydrates that do not contain sulphur (aluminium hydroxide and CAH₁₀), the influence of the
186 sulphur can be attributed
187 ○ to the change in the ionic strength of the solution that directly impacts activity coefficients
188 of the ions involved in the solubility products;

- o to the complex formation between Ca^{2+} and SO_4^{2-} in solution and
 - o to the lowering of OH^- concentration and consequently the decrease of the pore solution pH.

It should be noted that the OH^- is present in all the dissolution reactions and is coupled to pH via the equilibrium reaction $\text{H}_2\text{O} \rightleftharpoons \text{OH}^- + \text{H}^+$. For example the dissolution reactions of aluminium hydroxide and CAH_{10} are at high pH as follows:



The evolution of the pH in the two investigated scenarios is shown in Figure 3: left shows the pH map at the sulfate concentration of 0.1 mM and Figure 3-right at the sulfate concentration of 1 mM. The dissolution of Aluminium hydroxide is amphoteric and the equilibrium aluminium concentrations decrease strongly down to a pH of ~6.5 and then increases again at lower pH values. Figure 3 shows how higher sulphur concentrations decrease the pH of the solution, in particular at low Ca and Al concentrations. This decrease of solution pH strongly influences the solubility line of aluminium hydroxide and explains the observed increase at very low Ca concentrations where the pH values drop below 6. CAH₁₀ shows much less dependence on the sulphur concentrations as for the higher range of the Ca and Al concentrations pH is only moderately lowered.

- For hydrates that contain sulphur, the effect is more complex. Sulphur impacts not only ionic strength, complex formation and pH (OH^- concentration) but in addition the solubility product since the sulphur takes part in the dissolution reaction as shown below for ettringite:



On the one hand, increasing sulphur concentrations will push the solubility lines to lower Ca and Al concentrations because it is the part of the dissolution equation. On the other hand, increasing sulphur concentration lowers the OH^- concentration, which would shift the solubility lines to higher Ca and Al concentrations.

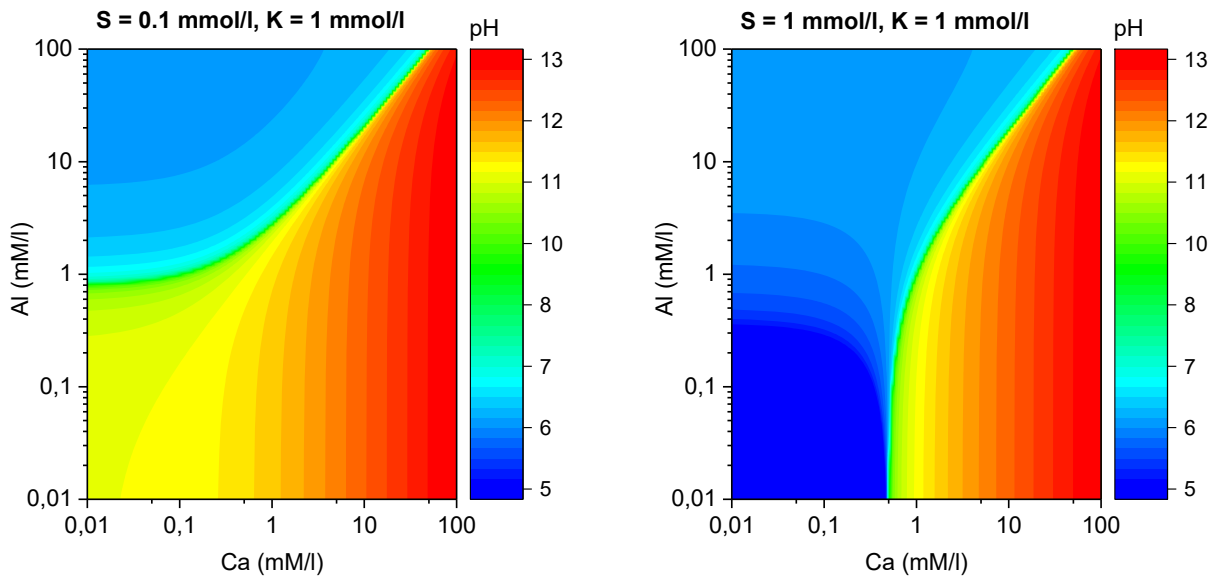


Figure 3 pH maps in the calcium alumina planes at the two sulphur levels 0.1 and 1 mM.

214

215 The effect of potassium on the solubility of the aluminium hydroxide, CAH_{10} phase and ettringite is shown in
 216 Figure 4. Potassium increases both the ionic strength of the solution as well as its pH. This results in higher
 217 aluminium concentrations in the presence of aluminium hydroxide and in a shift of the solubility line of
 218 ettringite to lower Ca and Al concentrations. The effect on CAH_{10} is non monotonic. At lower Ca concentration
 219 (< 3 mM), potassium lowers the Al concentrations. However, at high Ca concentrations (> 3 mM), more Al is
 220 expected in the presence CAH_{10} .

221

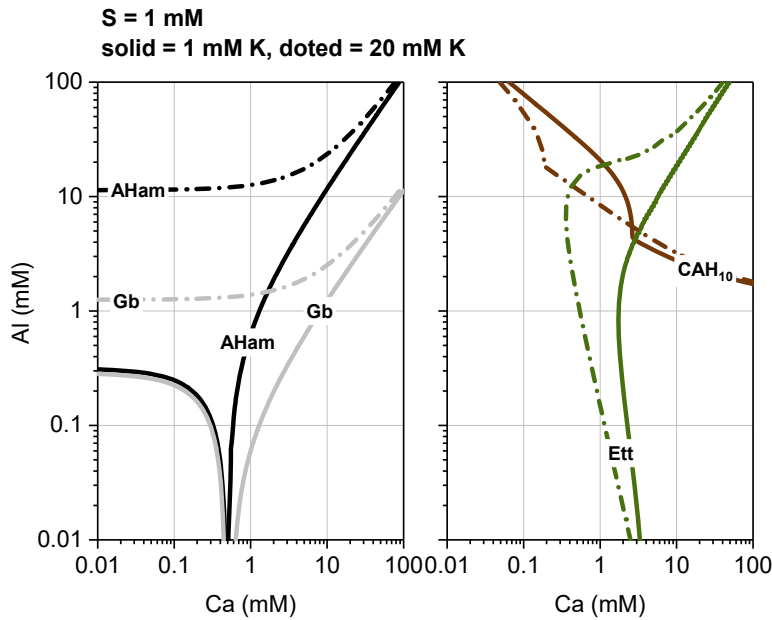


Figure 4 Solubility lines at different K concentrations: CAH₁₀ - CAH₁₀ phase, Ett – Ettringite, Gb – gibbsite, AHam - aluminium hydroxide amorphous. The solid line shown the calculation results at 1 mM of K, and doted 20 mM of K. Sulphur concentration is 1 mM in both cases.

222 **3.3. Three dimensional representation of the system**

223 As shown above the interactions in the pore solution in the Ca-Al-S-K-H₂O system are complex as the sulphur
 224 and potassium have a strong impact on the ionic strength, on complex formation and the pH of the solution.
 225 These in turn significantly affect the solubility lines even of sulfate-free hydrates. Since the dissolution of
 226 ye'elimit provides Ca, Al and sulphur to the solution, the analysis of solubility lines plotted in 2-dimensions
 227 cannot capture the complexity of these systems and plots in 3-dimensions showing solubility surfaces instead
 228 of lines are better suited. The three-dimensional diagram of solubility surfaces in the systems Ca-Al-S-H₂O is
 229 shown in Figure 5 in the range of 0.01 to 100 mM Ca, Al and sulphur at K = 1 mM. The surfaces for the phases
 230 Ett, aluminium hydroxide (gibbsite), CAH₁₀, C₂AH_{7.5}, and C₄AH₁₃ are shown as well as the theoretical
 231 dissolution line of stoichiometric ye'elimit. It is noticeable that solubility surfaces of Ett, C₂AH_{7.5}, and C₄AH₁₃
 232 are close to each other (note however the logarithmic scale) and their mutual distance as well as their
 233 crossings vary depending on the concentrations in the pore solution. Note that the solubility surface of
 234 monosulfate closely follows that of ettringite in the scenario modelled. The solubility surfaces of the
 235 remaining two hydrates, aluminium hydroxide and CAH₁₀, are distinctly different. While CAH₁₀ is

236 supersaturated only for high Al concentrations irrespective of those of calcium and sulphur, the solutions will
 237 be supersaturated with respect to aluminium hydroxide for practically any concentration, except at very high
 238 sulphur and calcium concentrations. Counter intuitively, the aluminium hydroxide solubility surface is the
 239 most complex one, inspite of there being no calcium or sulphur in aluminium hydroxide. The complex shape
 240 of the surface is a result of the interactions in the pore solution and their impact on pH. Note that the
 241 solubility surfaces of the different forms of aluminium hydroxide (amorphous, microcrystalline, crystalline)
 242 have a similar shape and are only 'shifted' along the vertical axis with aluminium concentration
 243 Additionally, Figure 5 shows that during the theoretical calculated dissolution of the ye'elimit in pure water,
 244 the solution is oversaturated with respect to several hydrates in the order aluminium hydroxide, CAH₁₀ and
 245 ettringite. Finally, the solution becomes supersaturated with the respect to the remaining hydrates
 246 investigated, if precipitation is not considered.

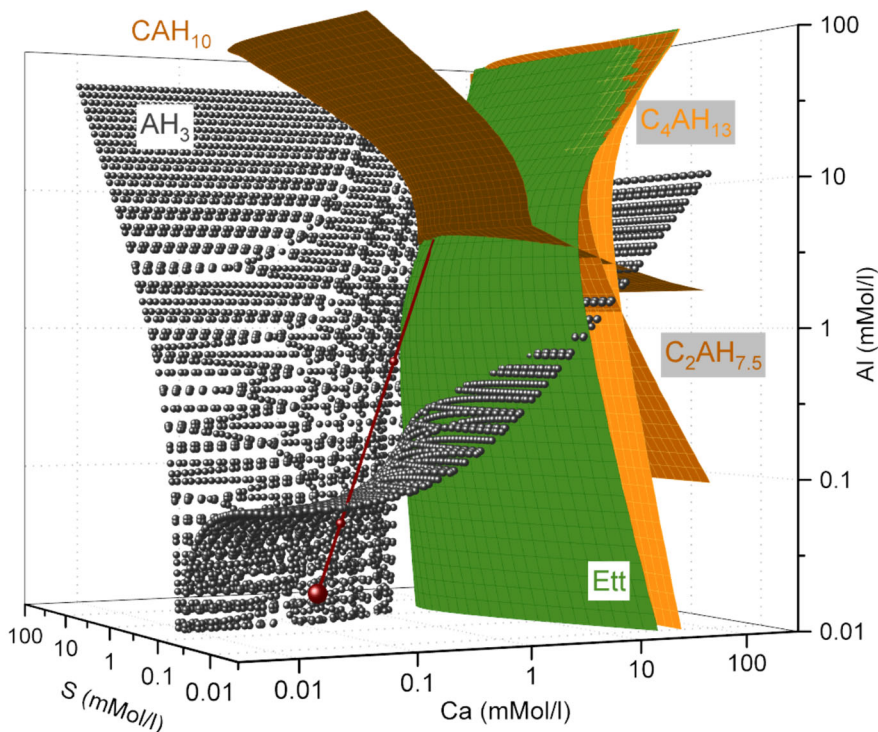


Figure 5 Solubility surfaces
for the system Ca-Al-S-H₂O.
K concentration is 1 mM.
The red line shows the
calculated change of the
concentrations as a result
of ye'elimit congruent
dissolution.

247
 248 So far, only generic results of the thermodynamic model have been considered and the complexity resulting
 249 from the interactions in multi-species solutions of high ionic strengths discussed. The key messages are
 250 following:

- 251 • Hydration reactions in Ca-Al-S-K-H₂O system cannot be analysed based on total concentrations and
252 a model accounting for speciation at high ionic strength is necessary.
253 • Solubility surfaces of phases are complex and highly dependent on activities of all ions including those
254 not involved in the solubility product equation.

255 At the initial stage of hydration, some phases such as aluminium hydroxide are very sensitive to even small
256 changes in alkali or sulphur concentrations.

257 **3.4. Reaction of ye'elimit in pure water**

258 In this section, the dissolution of ye'elimit is considered in detail to identify the stable hydrate domains and
259 how these are affected by the changing Ca, Al and sulphur concentrations. In addition, the relation between
260 the solubility surfaces and the evolution of the measured pore solution concentrations during the hydration
261 of ye'elimit are discussed. At the beginning of this section, the hydration of the pure ye'elimit is presented
262 shortly, based on earlier publication [9].

263 Figure 7 shows the evolution of the phase assemblage during the hydration of ye'elimit focussing on early
264 age. In these experiments, pure lab-synthesized ye'elimit and pure water were used [9], such that very low
265 alkali concentration of lower than 1 mM was present. Initially, ye'elimit reacts slowly, particularly up to
266 about 200 minutes. During this period, the main hydration products are ettringite and an XRD amorphous
267 phase. The reaction of Ye'elimit accelerates at about 500 minutes, the main hydration products observed
268 are monosulfate and XRD amorphous phase. Ye'elimit is fully hydrated at about 700 minutes. More detailed
269 description of the hydration process of ye'elimit is summarised e.g. in [9] and further extended in [10].

270

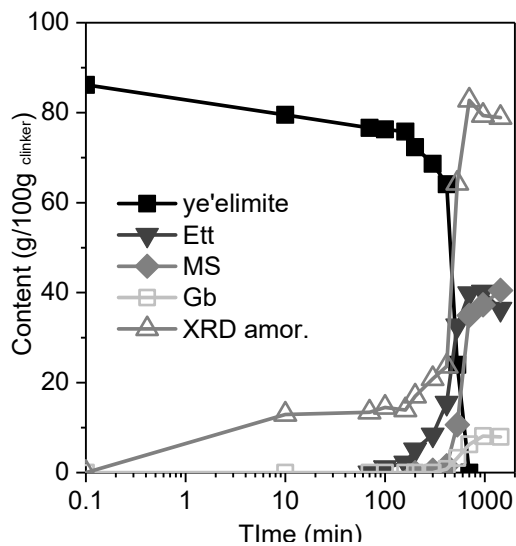


Figure 6 Evolution of the content of chosen phases during hydration of synthetic ye'elimite. Data replotted from [9].

271

272 Figure 7 shows the measured concentrations in the pore solution and calculated saturation indexes. The Ca,
 273 Al and sulphur concentrations increase in parallel up to about 90 minutes. During this period, little ye'elimite
 274 reaction is observed. Between 90 minutes and 400 minutes, the solution changes with strongly increasing Al
 275 concentration and a drop in sulphur. Finally, the concentrations decrease. The saturation indexes confirm
 276 that the main hydration products are ettringite and monosulphate as described above when discussing XRD
 277 data. Additionally, they suggest that the amorphous phase is composed of aluminium hydroxide and CAH₁₀
 278 phase [9].

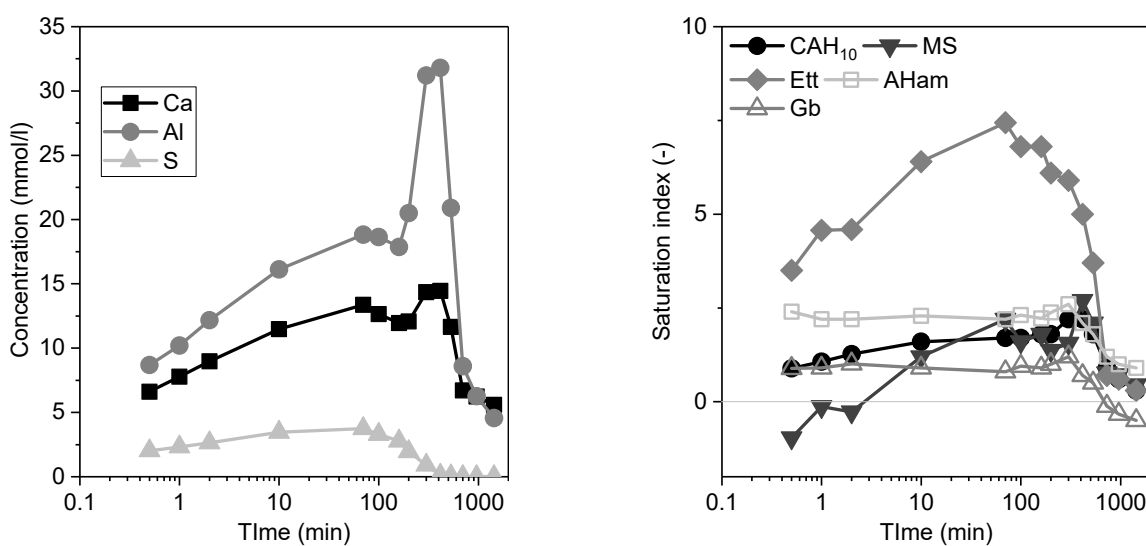


Figure 7 Pore solution concentrations measured during the reaction of ye'elimite at w/s = 40 in pure water.

Measured concentrations from [9]

279 In Figure 8 the measured pore solution concentrations from Figure 7 and [9] are compared with the
280 calculated solution concentration change during the pure dissolution of ye'elimit in pure water (indicated
281 by the red line) and the solubility surface of ettringite. The first measurements point (30 seconds) lies on the
282 calculated theoretical dissolution of ye'elimit indicating that the pore solution concentrations are changing
283 according to the theoretical dissolution line and no solids or a solid with a composition comparable to
284 ye'elimit have precipitated. The congruent dissolution path is followed up to about 90 minutes where
285 maximum solution concentrations of 15 mM Ca, 20 mM Al and 4 mM sulphur are reached.

286

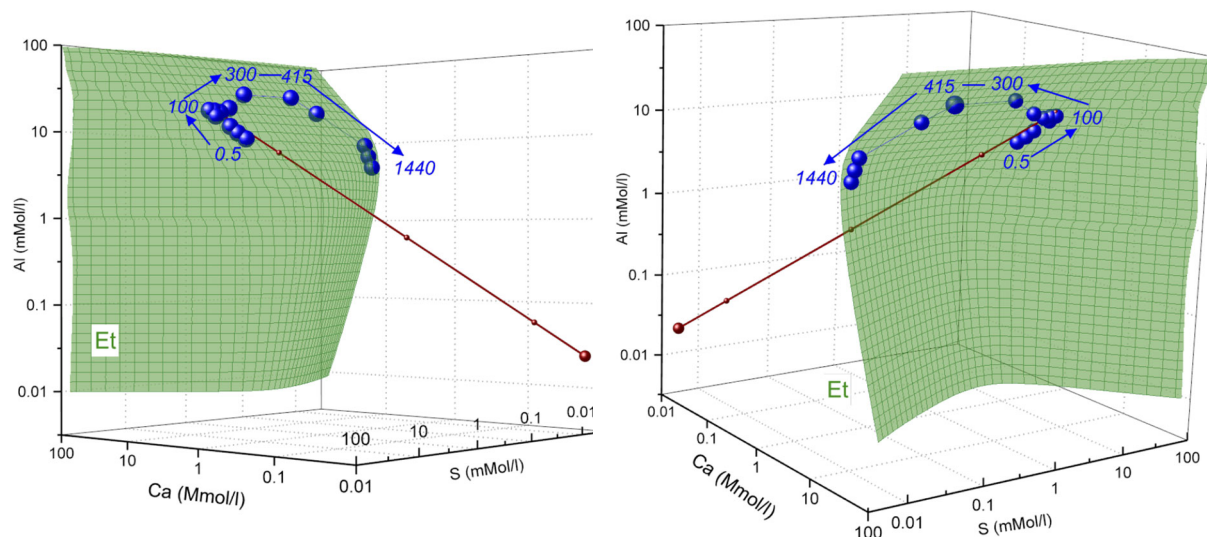


Figure 8 Solubility surface of ettringite calculated at 1 mM K compared to the theoretical dissolution line of ye'elimit (red) and measured concentrations of Ca, Al and S during the reaction of the synthetic, pure ye'elimit at w/c = 100 (blue points) [9]. The first measurement point is after 30 seconds. The arrows indicate the time evolution of the pore solution and the numbers the time of measurement in minutes. Both graphs show the same results but viewed from different perspective.

287

288 After 90 minutes, the concentrations deviate from the congruent dissolution line, indicating the formation
289 of a solid rich in calcium and sulfate. During the further reaction of ye'elimit, the measured pore solution
290 concentrations stay close to the surface of ettringite and other hydrates (Figure 8 and compare to [9]).

291 While the 3 D-graphs allow all surfaces at to be plotted at the same time, the level of complexity in such
 292 graphs is very high, consequently only intersections of surfaces from Figure 5 with different sulphur levels
 293 are plotted in Figure 9 to facilitate the discussion of the results. Additionally, the 2 D-graphs show all three
 294 crystallinities of aluminium hydroxide.

295

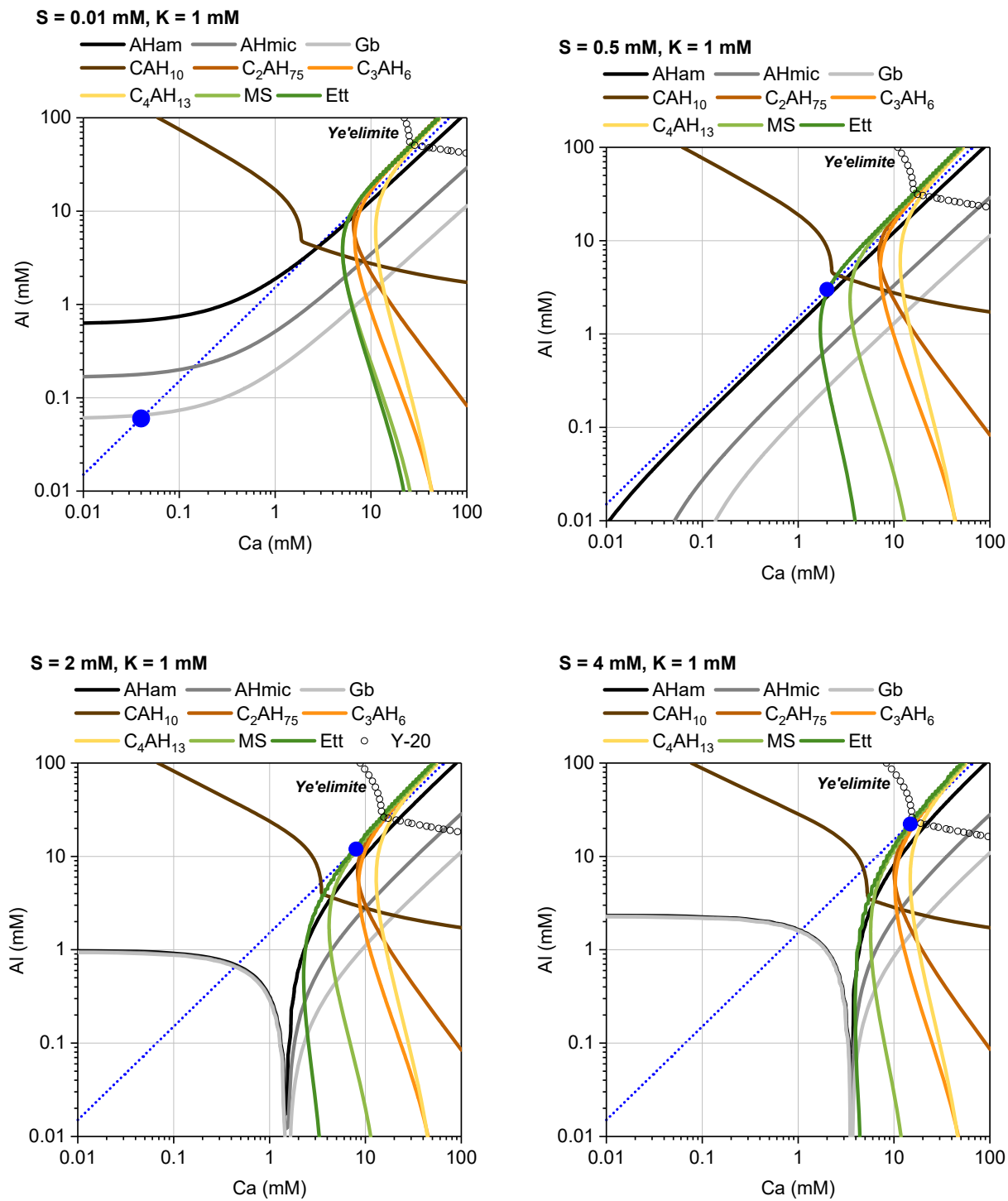


Figure 9 Intersections of surfaces from Figure 5 at different sulphur concentrations: CAH_{10} , $\text{C}_2\text{AH}_{7.5}$, C_3AH_6 , C_4AH_{13} , MS: monosulfate, Ett: Ettringite, Gb: gibbsite, AHmic – aluminium hydroxide microcrystalline, AHam - aluminium hydroxide amorphous. The straight dotted line shows the projection of theoretical congruent dissolution line of ye'elimitite on the Ca – Al plane. The blue circles depict the Ca and Al concentration corresponding to the concentration of S marked in the graph description. The plot at $S = 2 \text{ mM}$ corresponds to the first measurement point at 30 s from hydration starting. The plot at $S = 4 \text{ mM}$ corresponds to the point after ~90 minutes of the hydration. The ye'elimitite line (Y-20) depicts solubility of ye'elimitite decreased for 20 log units.

296

297 For the congruent dissolution of ye'elimitite , the concentrations of Al, Ca and S should increase continuously
298 as visualised by the blue dotted line in Figure 9, $S = 0.01$ to 4 mM , until solids start to precipitate. This
299 theoretical dissolution line first crosses the solubility line of gibbsite; however, the precipitation of this
300 crystalline phase is very slow at ambient temperature, so rather amorphous or microcrystalline aluminium
301 hydroxide forms [18]. The solubility lines of the microcrystalline and amorphous forms of aluminium
302 hydroxide would be crossed at very low sulphur concentrations. However, in parallel to the Al and Ca
303 concentration, also the sulphur concentration increases, which lowers the pH values and changes the
304 solubility lines of aluminium hydroxide as had been discussed above for Figure 2. Thus, the further increase
305 of the solution concentrations does not result in significant increases in supersaturation with respect to
306 amorphous aluminium hydroxide (Figure 9 $S = 0.5, 1$ and 4 mM) as the slope of the surface of AHam is similar
307 to the dissolution curve of ye'elimitite at sulphur concentrations larger than ~ 0.5 mM . At later times of
308 dissolution, i.e. at sulphur concentrations above 0.5 mM , the theoretical dissolution line of ye'elimitite crosses
309 the solubility line of ettringite followed by CAH_{10} phase. Further dissolution of ye'elimitite results in continuous
310 increases of the supersaturation against the CAH_{10} phase. However, the supersaturation with respect to
311 ettringite is limited because of the shape of its solubility surface almost parallel with the dissolution line
312 (compare with calculated SI in Figure 6). The experiments with a pure ye'elimitite ([9], Figure 7 and Figure 6)
313 demonstrate that the solution composition follows, after the first 90 minutes, the trend of the solubility
314 surface of ettringite, as also mirrored in the only moderate oversaturation of ettringite. Finally, it is noticeable
315 that during the first minutes of ye'elimitite dissolution, the undersaturation with respect to monosulfate

316 continuously increases. Only at the intermediate stages (after \sim 400 minutes) of the dissolution reaction
317 when the elements concentrations increase, monosulfate becomes oversaturated (corresponding to sulphur
318 concentration close to 4 mM). Gypsum is continuously undersaturated for all concentrations studied.
319 The shape of the solubility surfaces of the main hydrates is such that the continuous increase of the Al, Ca
320 and sulphur results in a relatively small increase of the supersaturation against the main hydrated phases
321 and thus in a relatively slow nucleation and precipitation, which explains the slow initial reaction of the
322 synthetic neat ye'elimit observed by calorimetry [9].
323 This low oversaturation occurs because gibbsite does not precipitate fast enough and only the amorphous
324 form of aluminium hydroxide precipitates to small extend during the first hours of ye'elimit reaction [9]. A
325 massive precipitation of gibbsite would deplete Al from the solution and the dissolution line would follow
326 the gibbsite surface instead of the congruent dissolution line in Figure 9. In such a case, the saturation
327 surfaces of ettringite and monosulfate would be crossed sooner (see Figure 9 at S = 2 and 4 mM) such that
328 the supersaturation with respect to ettringite and monosulfate would increase more rapidly leading to earlier
329 and more intense nucleation and precipitation of these two phases. A significant precipitation of CAH_{10}
330 (Figure 9, S = 2 and 4 mM) would have a similar effect, though less pronounced, and would lead to an earlier
331 nucleation and precipitation compared to the stoichiometric ye'elimit dissolution. In fact, the plot of the
332 experimental data and the congruent solubility curve illustrates that a small quantity of aluminium rich-
333 hydrates has precipitated [9] during the early hydration as shown in Figure 10. This lowers the aluminium
334 concentrations and results in a faster increase of the supersaturation which respect to the ettringite and later
335 on monosulfate than if no phase had precipitated.

336

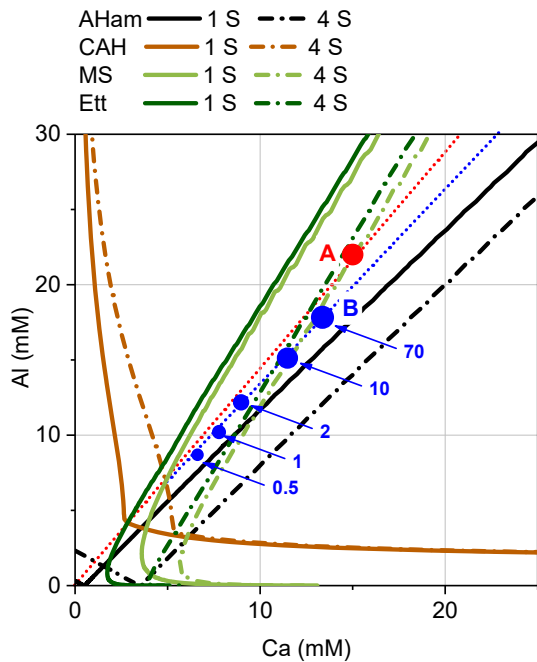


Figure 10 Intersections of surfaces of CAH - CAH₁₀, MS

– monosulfate, Ett – Ettringite, and AHam – aluminium hydroxide amorphous at 1 and 4 mM sulphur concentrations. The straight red dotted line shows the projection of theoretical dissolution line of ye'elimit on the Ca – Al plane. The blue points show the measured pore solution centration evolution during the first 70 minutes (numbers gives the measurement time). Point B shown the measured concentrations rat the highest sulphur level (~ 4 mM S) while point A represents the theoretical Ca and Al concentration assuming no precipitation.

337 Figure 11 shows the evolution of the measured pore solution concentrations between 90 minutes and 700
 338 minutes of hydration at w/b = 40. It is noticeable that the increase of the alumina concentration at the end
 339 of the dormant period is related to two phenomena:

- 340 • Hydrates precipitation leads to the accumulation of the alumina in pore solution, indicating the
 341 slower precipitation of AHam already discussed
- 342 • The decrease of the sulphur concentration increases the pH of the pore solution and the shape of
 343 the solubility surface such that monosulfate and ettringite continue to be supersaturated
- 344 • This increase of pH leads also to a change of the aluminium hydroxide solubility surfaces, such that
 345 after longer time the amorphous aluminium hydroxide becomes undersaturated and microcrystalline
 346 aluminium hydroxide starts to form (in agreement with occurrence of a more crystalline aluminium
 347 hydroxide as shown in Figure 7)

348

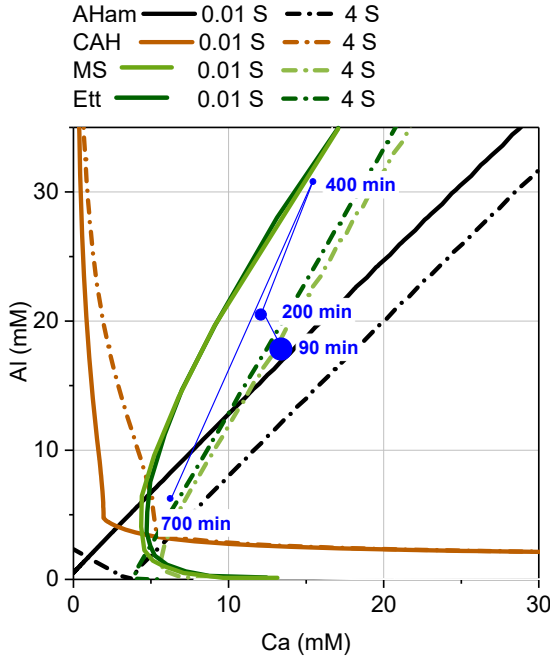


Figure 11 Intersections of surfaces of CAH - CAH_{10} , MS – monosulfate, Ett – Ettringite, and AHam - aluminium hydroxide amorphous at 0.01 and 4 mM sulphur concentrations.

The blue points show the measured pore solution concentration evolution during the measurement after 90 minutes at the highest sulphur level ($\sim 4 \text{ mM}$ sulphur). The other points represent the measured data after 200, 400 and 700 minutes and low sulphur concentrations ($\sim 0.01 \text{ mM}$ sulphur after 700 min).

349 3.5. Towards industrial cement

350 Until now, we have focused on the dissolution of neat stoichiometric ye'elimit and the effects caused by
 351 the interactions in the high ionic strength solution. Based on the changes to the saturation surfaces modelled,
 352 the sequence of events in the dissolving and hydrating systems could be explained. Even in this simpler case,
 353 the interactions were complex. Here we investigate in detail the dissolution of ye'elimit in the BYF clinker
 354 and the impact of reacting rapidly phases like alkali sulphates and C_{12}A_7 .

355 At the beginning of this section, the hydration of the BYF clinker is summarised, based on an earlier
 356 publication [20]. The evolution of the phase assemblage at the beginning of the hydration of BYF cement is
 357 dominated by the reaction of ye'elimit and principally similar to the pure ye'elimit as shown in Figure 12.
 358 It is noticeable that the dormant period is significantly shorter: ye'elimit starts to rapidly react after about
 359 120 minutes of hydration.

360

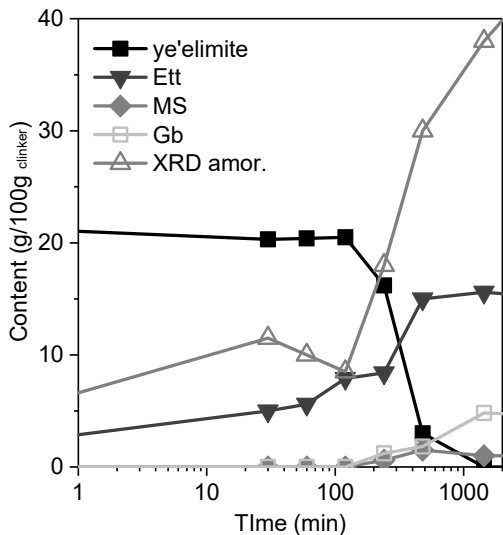


Figure 12 Evolution of the content of selected phases during BYF clinker hydration at w/b = 2. Data replotted from [20].

361
362 The pore solution evolution is shown in Figure 13. The evolution of the alumina concentration is similar to
363 that of pure ye'elimit, but with significantly higher concentration values. The concentrations of calcium and
364 sulphur are decreasing from the first measurement time, i.e. after 5 minutes from mixing with water. This
365 indicates, in contrast to the pure ye'elimit system discussed above, precipitation of calcium and sulphur rich
366 solids, consistent with the very early ettringite formation observed in these systems. Also, the sulphur
367 concentrations are significantly higher than observed for the ye'elimit reacting in pure water (c.f. Figure 7).
368 Additionally, the alkali concentration is high in industrial cements. The higher alkali concentration and high
369 initial sulphur concentrations are related to the alkali sulphates typically present in industrial and semi
370 industrial clinkers. Alkali sulphates dissolve almost instantly in mixing water leading to high alkali and sulphur
371 concentrations.

372

373

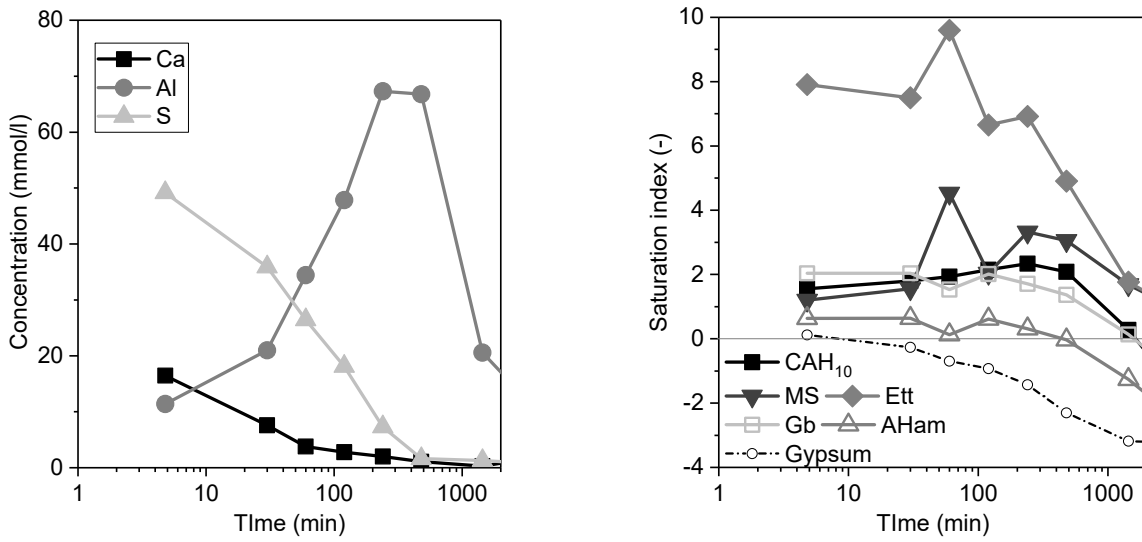


Figure 13 Pore solution concentrations measured during the reaction of BYF clinker at w/s = 2 in pure water.

Measured concentrations from [9].

374 These differences are also related to the presence of minor phases that are formed during the clinkering
 375 process and which significantly influence the hydration of ye'elimite in the cement. Calcium aluminate
 376 phases, CA and $C_{12}A_7$, are often present in laboratory and industrial clinkers [12][13][14][44][45][46].
 377 Particularly $C_{12}A_7$ reacts rapidly during the first minutes of the cement hydration [20][45][46] and has been
 378 shown to accelerate the kinetics of the ye'elimite hydration [10].

379

380 The effect of the presence of these phases on the dissolution process is explored in Figure 14 by plotting the
 381 pore solution composition against the solubility surfaces. The solubility surfaces are calculated for alkali and
 382 sulphur concentrations corresponding to data in Figure 13. In this work, the total alkali concentration at the
 383 first measurement time was about 100 mM and this corresponds to a sulphur concentration of 50 mM
 384 assuming they originate from readily soluble alkali sulphates. In order to simplify the analysis, we assumed
 385 that potassium is the only alkali present and that its content does not change during the early age hydration
 386 investigated. Again, the theoretical congruent dissolution curve of ye'elimite is plotted against the cross-
 387 section of the solubility surfaces of the main hydrates at the different sulphur levels is shown in Figure 14.
 388 The theoretical dissolution line of $C_{12}A_7$ phase has been added (red dotted line). This $C_{12}A_7$ dissolution line
 389 runs nearly parallel to the ye'elimite dissolution line.

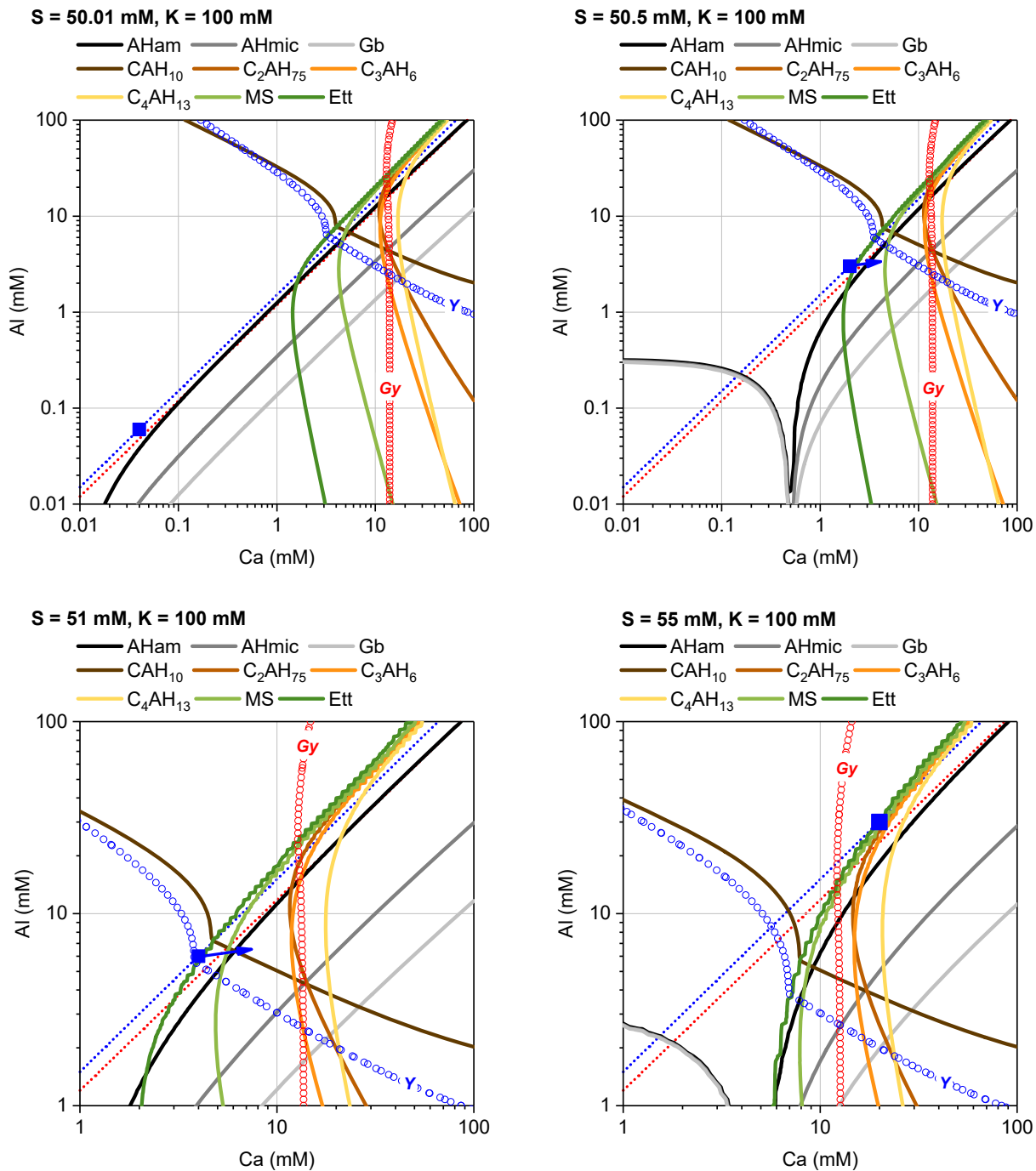


Figure 14 Intersections of solubility surfaces at different sulphur concentrations: Gy is the solubility surface of gypsum and Y is the ye'elimite solubility surface moved for 20 log units. In the calculation, an initial concentration of 50 mM K_2SO_4 was assumed.

The straight blue dotted line shows the theoretical congruent dissolution line of ye'elimite. The square blue points depict the Ca and Al concentration corresponding to the concentration of sulphur indicated on the graph. The straight red dotted line shows the Ca/Al ratio corresponding to the congruent, hypothetical dissolution of C_{12}A_7 phase. The arrow indicates the effect of C_{12}A_7 on the dissolution of ye'elimite.

390 The calculations reveals that the presence of 50 mM of K_2SO_4 in the solution (Figure 14) has a limited impact
391 on the calculated shape of the solubility surfaces of the calcium alumina hydrates compared to the case of
392 the dissolution of ye'elimit in pure water. The addition of only K_2SO_4 does not change the pH values
393 significantly when compare to the pure water (data not shown here). Only when more sulphur is added (so
394 the S/K is increased), which lowers the pH values, the curves show similar shifts as observed in Figure 9; thus
395 the concentration of sulphur of 0.01 mM in pure water corresponds to concentration of sulphur of 50.01 mM
396 in K_2SO_4 solution and 0.5 mM corresponds to 50.5 mM and so on.

397 There are two noticeable changes between the calculated solubility data for the pure water case and the
398 K_2SO_4 solution:

399 ○ Gypsum becomes supersaturated at higher calcium concentration for the case with K_2SO_4 in solution.
400 Note that in the Figure 9 gypsum was always under-saturated.
401 ○ At each investigated sulphur level, ye'elimit is less under saturated when compared to the
402 dissolution of the ye'elimit in the water.

403 The K_2SO_4 addition has a limited impact on the solubility lines of calcium alumina hydrates. Since the under-
404 saturation with respect to ye'elimit is lower at each sulphur level when compared to pure water case, its
405 reaction should be slower. However, the experiments provided in the literature show that ye'elimit reacts
406 significantly faster in the industrial cements; compare the kinetics of ye'elimit dissolution in Figure 6 and
407 Figure 12. The main reason for this acceleration is the $C_{12}A_7$ phase [10]. This phase has two pronounced
408 impacts on the calculated evolution of the pore solution during the dissolution of ye'elimit:
409 ○ The dissolution of $C_{12}A_7$ increases the Al and Ca concentration relative to the sulphur released from
410 ye'elimit.
411 ○ It moves the dissolution curve of the ye'elimit towards lower aluminium and higher calcium
412 concentrations as shown by the red dotted line in Figure 14,
413 These specific effects are confirmed by the pore solution concentrations measured during the dissolution of
414 ye'elimit in the presence on $C_{12}A_7$ as discussed in detail in [10]. These phenomena have a pronounced
415 impact on the development of the pore solution concentration relative to the solubility surfaces during the

416 dissolution ye'elite in the cement clinker. At any given quantity of the ye'elite dissolved, i.e. at the given
417 increase of the sulphur concentration in Figure 14, the solution is always more supersaturated initially with
418 respect to aluminium hydroxide and later on with respect to ettringite and CAH₁₀. Hence these phases can
419 precipitate earlier and faster. It is also noticeable that the presence of C₁₂A₇ results in a different order in
420 which the solubility surfaces are crossed during the ye'elite dissolution. While in the case of pure ye'elite
421 (Figure 9), the solution is supersaturated with respect to aluminium hydroxide and later on with respect to
422 CAH₁₀ and ettringite, the presence of C₁₂A₇ and alkali sulfates in industrial clinkers modifies the pore solution
423 composition such that it is first supersaturated with respect to ettringite and later on with respect to CAH₁₀.
424 Overall, these changes contribute to the acceleration of ye'elite hydration in the industrial cements
425 compared to the reaction of neat ye'elite in pure water.

426 Another interesting point is the effect of alkalis on the evolution described above. The alkalis present as alkali
427 sulphate and those dissolved in the rapidly hydrating clinker phases (e.g. ye'elite [27]) dissolve rapidly
428 during the first minutes of the cement hydration, which increases the pH of the pore solution and affects the
429 shape of the solubility surfaces. It should be noted that in the semi industrial and industrial cements the pH
430 of the pore solution is about 1 unit higher at all stages of the hydration than in the synthetic ye'elite
431 dissolving in water (compare the data in [9], [10], [20], [25]). The effect of the alkali dissolution is shown in
432 Figure 15 for two S concentrations of 50.5 and 55 mM, respectively.

433

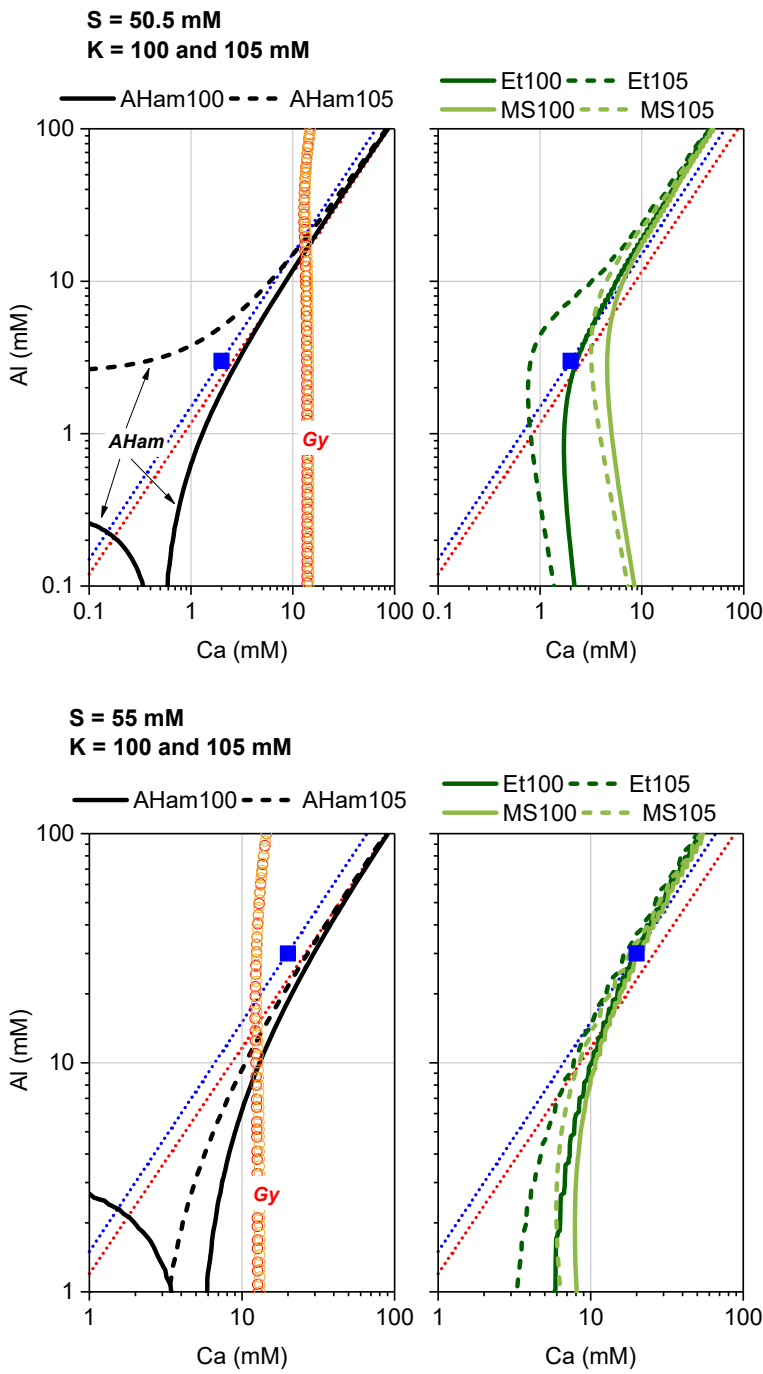


Figure 15 Intersections of solubility surfaces at $S = 50.5$ and 55 mM and two K concentrations equal to 100 and 105 mM. The straight blue dotted line shows the projection of theoretical dissolution line of ye'elimit on the $\text{Ca} - \text{Al}$ plane. The square blue points depict the Ca and Al concentration corresponding to $S = 0.5$ at 1 mM from ye'elimit. The straight red dotted line shows the Ca/Al ratio corresponding to the dissolving C_{12}A_7 phase.

434

435 For this comparison the solubility surfaces were calculated at the alkali level $K = 105$ mM and compared to
436 the 100 mM as shown in Figure 15. It is noticeable that the increasing alkali concentration modifies the shape

437 of the solubility of ettringite and monosulfate in such way that they are crossed earlier and the
438 supersaturation increases more rapidly during the calculated dissolution of ye'elimit. Contrary, the solubility
439 surface of aluminium hydroxide is modified in the way that the solution is initially undersaturated with
440 respect to this phase at the higher alkali level. This can further contribute to the acceleration of the ye'elimit
441 hydration in industrial cement when compared to the pure ye'elimit reaction. It is important to notice that
442 the solubility surface of the gypsum is not significantly modified.

443 **4. Conclusions**

444 Thermodynamic modelling is a powerful tool to determine the variation of the system in presence of
445 solutions having known compositions. A knowledge of the equilibrium diagram is important even if the
446 system is dynamic (not at equilibrium) as occurs at the beginning of hydration: in fact it enables the kinetic
447 path of the reaction to be traced and so to determine if the solution is supersaturated or undersaturated
448 with respect to stable (or metastable hydrates if the metastable system is calculated) as mention already in
449 the 90s by Damidot and Glasser [30], [31] [32].

450 Contrary to previous studies on CAC and calcium silicates – the speciation model for high ionic strength
451 solutions enabled us to study the Ca-Al-S-K-H₂O system accounting for complex interactions in the pore
452 solution. By comparing the solubility surfaces with experimentally determined pore solution concentrations,
453 it is demonstrated that the hydration pathways follow the stability fields of certain hydrates.

454 For hydration of stoichiometric synthetic ye'elimit, the evolution of the pore solution concentrations
455 observed could be explained. During the initial dormant period, the saturation with respect to calcium
456 bearing hydrates changes significantly less than the changes of the concentrations would suggest. This is
457 caused by the interactions among the sulphur-bearing ionic species with alumina and calcium-bearing ones,
458 making the saturation surfaces almost parallel to the congruent dissolution line of ye'elimit. Once hydrates
459 start to precipitate, their supersaturation does not change as dramatically as the pore solution concentration.
460 Again, this is caused by the specific impact of the pore solution composition on the solubility of the involved
461 phases.

462 The same framework was successfully applied to the early hydration of industrial calcium sulfo-aluminates
463 cements and shows how the presence of alkalis and C₁₂A₇ can accelerate the kinetics of ye'elimitite hydration.
464 While the alkalis from soluble salts such as (Na,K)SO₄ have little impact on the hydration path, alkalis
465 dissolved in clinker forming phases move the solubility surfaces of the hydrated phases towards lower
466 concentrations of Ca, Al and sulphur which accelerates the hydration process. A similar impact could be
467 associated with the presence and dissolution of C₁₂A₇ from clinker.
468 The qualitative as well as quantitative agreement of the modelling results with the experimental data and
469 observations not only proves the applicability of thermodynamic modelling to assessment of the hydration
470 of calcium sulfo-aluminates, but also enables identification of the mechanisms involved which leads, finally,
471 to a predictive model for the hydration pathways depending on the initial conditions and material
472 compositions.

473 **5. References**

- 474 [1] F. P. Glasser and L. Zhang, "High-performance cement matrices based on calcium sulfoaluminate–belite
475 compositions," *Cement and Concrete Research*, vol. 31, no. 12, pp. 1881–1886, 2001.
476 [2] M. C. G. Juenger, F. Winnefeld, J. L. Provis, and J. H. Ideker, "Advances in alternative cementitious
477 binders," *Cement and Concrete Research*, vol. 41, no. 12, pp. 1232–1243, Dec. 2011.
478 [3] T. Sui, "Progress and future perspectives of CSA cements in China," in *International Workshop on
479 Calcium Sulfoaluminate cements*, Murten, Switzerland, 2018.
480 [4] E. M. Gartner and D. E. Macphee, "A physico-chemical basis for novel cementitious binders," *Cement
481 and Concrete Research*, vol. 41, no. 7, pp. 736–749, Jul. 2011.
482 [5] E. Gartner and H. Hirao, "A review of alternative approaches to the reduction of CO₂ emissions
483 associated with the manufacture of the binder phase in concrete," *Cement and Concrete Research*, vol.
484 78, pp. 126–142, Dec. 2015.
485 [6] W. Dienemann, D. Schmitt, F. Bullerjahn, and M. B. Haha, "Belite-Calciumsulfoaluminate-Ternesite
486 (BCT)-a new low carbon clinker technology," *Cement International*, vol. 11, no. 4, pp. 100–109, 2013.
487 [7] J. Skocek, M. Zajac, B. Bullerjahn, and M. Ben Haha, "Effect of retarders on the early performance of
488 CSA-type cement," *19th Ibausil. Weimar, Germany*, 2015.
489 [8] M. Zajac, J. Skocek, C. Stabler, F. Bullerjahn, and M. Ben Haha, "Hydration and performance evolution
490 of belite–ye'elimitite–ferrite cement," *Advances in Cement Research*, pp. 1–14, Sep. 2018.
491 [9] F. Bullerjahn, E. Boehm-Courjault, M. Zajac, M. Ben Haha, and K. Scrivener, "Hydration reactions and
492 stages of clinker composed mainly of stoichiometric ye'elimitite," *Cement and Concrete Research*, vol.
493 116, pp. 120–133, Feb. 2019.
494 [10] F. Bullerjahn, M. Zajac, M. Ben Haha, and K. L. Scrivener, "Factors influencing the hydration kinetics of
495 ye'elimitite; effect of mayenite," *Cement and Concrete Research*, vol. 116, pp. 113–119, Feb. 2019.
496 [11] F. Winnefeld and B. Lothenbach, "Phase equilibria in the system Ca₄Al₆O₁₂SO₄–Ca₂SiO₄–CaSO₄–H₂O referring to the hydration of calcium sulfoaluminate cements," *RILEM Technical Letters*, vol. 1,
497 pp. 10–16, 2016.
498

- 499 [12] S. Berger, C. Cau Dit Coumes, P. Le Bescop, and D. Damidot, "Hydration of calcium sulfoaluminate
500 cement by a ZnCl₂ solution: Investigation at early age," *Cement and Concrete Research*, vol. 39, no. 12,
501 pp. 1180–1187, Dec. 2009.
- 502 [13] S. Berger, C. C. D. Coumes, P. Le Bescop, and D. Damidot, "Influence of a thermal cycle at early age on
503 the hydration of calcium sulfoaluminate cements with variable gypsum contents," *Cement and
504 Concrete Research*, vol. 41, no. 2, pp. 149–160, Feb. 2011.
- 505 [14] P. Wang, N. Li, and L. Xu, "Hydration evolution and compressive strength of calcium sulphoaluminate
506 cement constantly cured over the temperature range of 0 to 80 °C," *Cement and Concrete Research*,
507 vol. 100, pp. 203–213, Oct. 2017.
- 508 [15] D. Gastaldi *et al.*, "Hydration products in sulfoaluminate cements: Evaluation of amorphous phases by
509 XRD/solid-state NMR," *Cement and Concrete Research*, vol. 90, pp. 162–173, Dec. 2016.
- 510 [16] F. Song, Z. Yu, F. Yang, Y. Lu, and Y. Liu, "Microstructure of amorphous aluminum hydroxide in belite-
511 calcium sulfoaluminate cement," *Cement and Concrete Research*, vol. 71, pp. 1–6, May 2015.
- 512 [17] Y. Zhang and J. Chang, "Microstructural evolution of aluminum hydroxide gel during the hydration of
513 calcium sulfoaluminate under different alkali concentrations," *Construction and Building Materials*, vol.
514 180, pp. 655–664, Aug. 2018.
- 515 [18] B. Lothenbach, L. Pelletier-Chaignat, and F. Winnefeld, "Stability in the system CaO–Al₂O₃–H₂O,"
516 *Cement and Concrete Research*, vol. 42, no. 12, pp. 1621–1634, Dec. 2012.
- 517 [19] D. Jansen, A. Spies, J. Neubauer, D. Ectors, and F. Goetz-Neunhoeffer, "Studies on the early hydration
518 of two modifications of ye'elimit with gypsum," *Cement and Concrete Research*, vol. 91, pp. 106–116,
519 2017.
- 520 [20] M. Zajac, J. Skocek, F. Bullerjahn, and M. Ben Haha, "Effect of retarders on the early hydration of
521 calcium-sulpho-aluminate (CSA) type cements," *Cement and Concrete Research*, vol. 84, pp. 62–75, Jun.
522 2016.
- 523 [21] V. Morin, P. Termkhajornkit, B. Huet, and G. Pham, "Impact of quantity of anhydrite, water to binder
524 ratio, fineness on kinetics and phase assemblage of belite-ye'elimit-ferrite cement," *Cement and
525 Concrete Research*, vol. 99, pp. 8–17, Sep. 2017.
- 526 [22] L. Zhang and F. P. Glasser, "Hydration of calcium sulfoaluminate cement at less than 24 h," *Advances in
527 Cement Research*, Oct. 2002.
- 528 [23] J.-B. Champenois *et al.*, "Influence of sodium borate on the early age hydration of calcium
529 sulfoaluminate cement," *Cement and Concrete Research*, vol. 70, pp. 83–93, Apr. 2015.
- 530 [24] C. Cau Dit Coumes, M. Dhouri, J.-B. Champenois, C. Mercier, and D. Damidot, "Combined effects of
531 lithium and borate ions on the hydration of calcium sulfoaluminate cement," *Cement and Concrete
532 Research*, vol. 97, pp. 50–60, Jul. 2017.
- 533 [25] F. Winnefeld and B. Lothenbach, "Hydration of calcium sulfoaluminate cements — Experimental
534 findings and thermodynamic modelling," *Cement and Concrete Research*, vol. 40, no. 8, pp. 1239–1247,
535 Aug. 2010.
- 536 [26] J. Wang, I. Baco, V. Morin, G. Walenta, D. Damidot, and E. Gartner, "Hydration mechanism of cements
537 based on low-CO₂ clinkers containing belite,ye_elimit and calcium.pdf," in 2010, At Jinan, China, 2010,
538 vol. Session 1.
- 539 [27] F. Bullerjahn, "Characterisation and hydration of ye'elimit containing cements," EPFL, 2018.
- 540 [28] K. L. Scrivener and A. Nonat, "Hydration of cementitious materials, present and future," *Cement and
541 concrete research*, vol. 41, no. 7, pp. 651–665, 2011.
- 542 [29] D. Damidot, B. Lothenbach, D. Herfort, and F. P. Glasser, "Thermodynamics and cement science,"
543 *Cement and Concrete Research*, vol. 41, no. 7, pp. 679–695, Jul. 2011.
- 544 [30] D. Damidot and F. P. Glasser, "Thermodynamic investigation of the CaO-Al₂O₃-CaSO₄-K₂O-H₂O system
545 at 25° C," *Cement and concrete research*, vol. 23, no. 5, pp. 1195–1204, 1993.
- 546 [31] D. Damidot and F. P. Glasser, "Thermodynamic investigation of the CaO-Al₂O₃-CaSO₄-H₂O system at
547 25° C and the influence of Na₂O," *Cement and Concrete Research*, vol. 23, no. 1, pp. 221–238, 1993.
- 548 [32] D. Damidot and F. Glasser, "Investigation of the CaO-Al₂O₃-SiO₂-H₂O system at 25 C by thermodynamic
549 calculations," *Cement and Concrete Research*, vol. 25, no. 1, pp. 22–28, 1995.

- 550 [33] W. Hummel, U. Berner, E. Curti, F. Pearson, and T. Thoenen, "Nagra/PSI chemical thermodynamic data
551 base 01/01," *Radiochimica Acta*, vol. 90, no. 9-11/2002, pp. 805–813, 2002.
- 552 [34] W. Hummel, U. Berner, E. Curti, F. Pearson, and T. Thoenen, "Nagra Technical Report NTB 02-16,"
553 *Wettingen, Switzerland*, 2002.
- 554 [35] T. Matschei, B. Lothenbach, and F. P. Glasser, "Thermodynamic properties of Portland cement hydrates
555 in the system CaO–Al₂O₃–SiO₂–CaSO₄–CaCO₃–H₂O," *Cement and Concrete Research*, vol. 37, no. 10,
556 pp. 1379–1410, Oct. 2007.
- 557 [36] B. Lothenbach *et al.*, "Cemdata18: A thermodynamic database for hydrated Portland cements and
558 alkali-activated materials," *Cement and Concrete Research*, in press 2018.
- 559 [37] D. A. Kulik *et al.*, "GEM-Selektor geochemical modeling package: revised algorithm and GEMS3K
560 numerical kernel for coupled simulation codes," *Computational Geosciences*, vol. 17, no. 1, pp. 1–24,
561 2013.
- 562 [38] T. Wagner, D. A. Kulik, F. F. Hingerl, and S. V. Dmytrieva, "GEM-Selektor geochemical modeling package:
563 TSolMod library and data interface for multicomponent phase models," *The Canadian Mineralogist*,
564 vol. 50, no. 5, pp. 1173–1195, 2012.
- 565 [39] W. Wang, X. Chen, Y. Chen, Y. Dong, and C. Ma, "Calculation and verification for the thermodynamic
566 data of 3CaO·3Al₂O₃·CaSO₄," *Chinese Journal of Chemical Engineering*, vol. 19, no. 3, pp. 489–495,
567 2011.
- 568 [40] J. Wang, "Le mécanisme d'hydratation de ciment basé aux mâchefers Bas-CO₂ contenant belite,
569 ye'elite et l'alumino-ferrite de calcium," Université des Sciences et Technologie de Lille-Lille I, 2010.
- 570 [41] P. Barret, D. Bertrandie, and D. Beau, "Calcium hydrocarboaluminate, carbonate, alumina gel and
571 hydrated aluminates solubility diagram calculated in equilibrium with CO₂g and with Naaq+ ions,"
572 *Cement and concrete research*, vol. 13, no. 6, pp. 789–800, 1983.
- 573 [42] F. M. Lea and P. C. Hewlett, *Lea's chemistry of cement and concrete*. Elsevier, 2004.
- 574 [43] G. Le Saout, "Calcium aluminate based hydraulic binders: a review," in *Conference: 2nd International
575 conference on the chemistry of construction materials*, Munisch, Germany, 2016, vol. 50.
- 576 [44] L. H. J. Martin, F. Winnefeld, E. Tschopp, C. J. Müller, and B. Lothenbach, "Influence of fly ash on the
577 hydration of calcium sulfoaluminate cement," *Cement and Concrete Research*, vol. 95, pp. 152–163,
578 May 2017.
- 579 [45] M. C. Martín-Sedeño *et al.*, "Aluminum-rich belite sulfoaluminate cements: Clinkering and early age
580 hydration," *Cement and Concrete Research*, vol. 40, no. 3, pp. 359–369, Mar. 2010.
- 581 [46] F. Bullerjahn, D. Schmitt, and M. Ben Haha, "Effect of raw mix design and of clinkering process on the
582 formation and mineralogical composition of (ternesite) belite calcium sulphoaluminate ferrite clinker,"
583 *Cement and Concrete Research*, vol. 59, pp. 87–95, May 2014.

584
585